

Supplementary Appendix

This appendix has been provided by the authors to give readers additional information about their work.

Supplement to: Simsek Kiper PO, Saito H, Gori F, et al. Cortical-bone fragility — insights from sFRP4 deficiency in Pyle's disease. *N Engl J Med* 2016;374:2553-62. DOI: 10.1056/NEJMoa1509342

APPENDIX

TABLE OF CONTENTS

- List of Investigators and Affiliations
- Methods
- Supplementary Figures and Tables
- Supplementary Figure Legends
- Supplementary References

LIST OF INVESTIGATORS AND AFFILIATIONS

Pelin Ozlem Simsek Kiper M.D.*, Hiroaki Saito, Ph.D.*, Francesca Gori Ph.D.*, Sheila Unger M.D. Eric Hesse M.D., Ph.D., Kei Yamana Ph.D., Riku Kiviranta M.D., Ph.D., Nicolas Solban Ph.D., Jeff Liu M.D., Robert Brommage Ph.D., Koray Boduroglu M.D., Ph.D., Luisa Bonafé M.D., Belinda Campos-Xavier Ph.D., Esra Dikoglu M.D., Richard Eastell M.D., Fatma Gossiel M.D., Keith Harshman Ph.D., Gen Nishimura M.D., Katta Mohan Girisha M.D., Brian J. Stevenson Ph.D., Hiroyuki Takita M.D., Carlo Rivolta Ph.D. , Andrea Superti-Furga M.D.¶, Roland Baron D.D.S., Ph.D.¶

The authors' affiliations are as follows:From the Center for Molecular Diseases (P.O.S.K., L.B.,B.C.-X., E.D.), Medical Genetics Service (S.U.), and Department of Pediatrics (A.S.-F.), Lausanne University Hospital, the Genomic Technologies Facility, Center for Integrative Genomics (K.H.), and Department of Computational Biology, Unit of Medical Genetics (C.R.), University of Lausanne, and the Swiss Institute of Bioinformatics (B.S.) — all in Lausanne, Switzerland; the Unit of Pediatric Genetics, Department of Pediatrics, Hacettepe University Medical Faculty, Ankara, Turkey (P.O.S.K., K.B.); Harvard School of Dental Medicine, Department of Oral Medicine, Infection and Immunity (H.S., F. Gori, E.H., K.Y.,R.K., R. Baron), and Harvard Medical School, Department of Medicine, Endocrine Unit, Massachusetts General Hospital (R. Baron) — both in Boston; Acceleron Pharma, Cambridge, MA (N.S.); Lexicon Pharmaceuticals, The Woodlands, TX (J.L., R. Brommage); Academic Unit of Bone Metabolism, Metabolic Bone Centre Northern General Hospital, Sheffield, United Kingdom (R.E., F. Gossiel); Department of Radiology and Medical Imaging, Tokyo Metropolitan Kiyose Children's Hospital, Kiyose (G.N.), and Department of Orthopedics, National Hospital Organization Saga Hospital, Saga (H.T.) — both in Japan; and the Department of Medical Genetics, Kasturba Medical College, Manipal University, Manipal, India (K.M.G.)

*These Authors contributed equally.

¶Joint senior and corresponding Authors.

Current addresses: Hiroaki Saito and Eric Hesse: University Medical Center Hamburg-Eppendorf, Hamburg, Germany; Kei Yamana: Teijin Institute for Biomedical Research, Teijin Pharma Limited, Hino Tokyo, Japan. Riku Kiviranta: Department of Medical Biochemistry and Genetics and Department of Medicine, University of Turku, Turku, Finland.

METHODS

Molecular analysis

Fragmented genomic DNA was purified with AMPure XP beads and its quality was assessed with an Agilent Bioanalyzer. Preparation of the exome enriched, barcoded sequencing libraries was performed using the SureSelect Human All Exon v4 kit (Agilent). The final libraries were quantified with a Qubit Fluorometer (Life Technologies) and the correct size distribution was validated on the Agilent Bioanalyzer. Libraries were then sequenced on a HiSeq 2000 machine (Illumina), generating 100 bp paired-end reads. Raw reads were aligned onto the hg19 reference genome using Novoalign (<http://www.novocraft.com>). Data cleanup and variant calling were performed according to GATK Best Practices recommendations ¹. Variant filtering was made with Annovar ² and with in-house *perl* and *bash* scripts, available upon request. Homozygosity mapping was achieved by the use of the HomozygosityMapper software ³ on the merged *vcf* file of the two patients. A comparison was made between the two affected sibs (cases) and the reference genome (control) in order to detect regions of autozygosity shared by the two sibs. Filtering of exome variants was done for rarity (variant frequency = 1% or less in public databases), putative pathogenicity (variants seen at homozygosity in public databases (ExAC) were excluded), and quality (WES data with less than 15 reads per nucleotide and genotype quality less than 50, as well as variants present in other WES processed in-house by the same pipeline to remove technical error). Furthermore, variants were prioritized according to their presence in both affected sibs as well as for their location in regions of homozygosity by descent. Three variants were retained after this filtering procedure; a Tyr-to-Cys change (c.1067A>G/p.Y356C) in the *C9* gene coding for

complement component 9, an Arg-to-Gln change (c.2006G>A/p.R669Q) in the *DAB2* gene coding for a mitogen-responsive phosphoprotein, and a single nucleotide insertion predicting a frameshift with early truncation (c.498_499insG /p.Asp167Glyfs*3) in the *SFRP4* gene coding for soluble frizzled-related protein 4.

Quantification of SFRP4-specific mRNA in cultured fibroblasts isolated from patient 2.

Total RNA from confluent fibroblast cultures was purified using a commercial kit (QIAamp RNA blood mini, Qiagen) and retrotranscribed, and cDNA-specific primers (spanning from exon 4 to exon 6; sequences available upon request) were used to amplify a 149 bp of the *SFRP4* cDNA. GAPDH cDNA was amplified as internal reference. The quantitative PCRs were performed using the Rotor-gene SYBR Green kit (Quiagen) in a Rotor-Gene 6000 apparatus (Corbett). The *SFRP4/GAPDH* ratio in control cells was set as 100% and the results in the cells from patient 2 were expressed as percentage compared to the reference value.

Animals. Two lines of knockout mice with disruption of the first exon of the *Sfrp4* gene were independently generated at Lexicon (The Woodlands, Texas, USA) and Procter & Gamble (Cincinnati, Ohio, USA). Both mouse lines, analyzed at Lexicon and at Harvard, respectively, developed identical skeletal phenotypes. For all studies *Sfrp4*^{+/-} mice were interbred to obtain *Sfrp4*^{+/+} (*wt*), *Sfrp4*^{+/-}, and *Sfrp4*^{-/-} mice. 5 to 6 mice for group were analyzed. All animal protocols were approved by the Harvard Medical School Institutional Animal Care and Use Committee policies. Bone histomorphometry and microCT (μ CT) analysis were done blindly.

Skeletal analyses. *Sfrp4*^{+/+} (*wt*), *Sfrp4*^{+/-} and *Sfrp4*^{-/-} mice were sacrificed at the age of 1, 3, 4, 7, 10, and 17, 24, 44, 60 and 68 weeks. Limbs from 8 days old mice were fixed in 4% PFA followed by decalcification, dehydration and paraffin embedding. Tissue blocks were cut

into 6 μm sections, deparaffinized and rehydrated. Sections were stained with Hematoxylin & Eosin (H&E) to permit phenotypic analyses or with TRAP to count osteoclast number following the same protocols used for bone histomorphometry. Dynamic and cellular bone histomorphometry was performed on 10 and 44 week-old mice. Animals were injected 8 days and 2 days prior to sacrifice with calcein (20 mg/kg body weight) and demeclocycline (20 mg/kg body weight) (both Sigma). For phenotype analyses, tibiae were fixed in 3.7% PBS-buffered formaldehyde and embedded in methylmethacrylate. Toluidine blue and von Kossa stains were performed using 5 μm saggital sections. Quantitative bone histomorphometric measurements were performed according to standardized protocols⁴ using the OsteoMeasure system (OsteoMetrics). Cortical remodeling and thickness in longitudinal von Kossa-stained or non-stained sections of the tibiae were measured by using the proximal tibio-fibular junction as a precise anatomical landmark for embedding and sectioning. Cortical histomorphometry was performed over a 450 microns high area that covers both cortices and that starts 4.5 mm below the middle of the proximal tibio-fibular junction. Cellular activities, fluorescent labels and thickness were calculated according to the area and surfaces included in the 450 microns high box. All histological images were obtained at room temperature using a microscope (Eclipse E800; Nikon) with 20x (no medium; NA 0.50) objective fitted with a camera (DP71, Olympus) and software (DP controller; Olympus). To assess the effect of RAP-661 and Scl-Ab treatments on the bone diameter, bone diameter was measured starting 3 mm above the distal junction of fibula/ tibia. The length of measured area was 1mm. Three-dimensional bone architecture was determined by μCT using a Scanco $\mu\text{CT}40$ employing a threshold of 240, an X-ray tube voltage of 55 keV, a current of 145 μA and an integration time of 200 μs . Voxel dimensions for each study are provided in the table and figure legends. For cortical bone analyses in the femur (midshaft) and tibia (tibia-fibula junction), twenty slices were analyzed and total area of bone plus marrow was determined as an estimate of bone diameter. For mechanical test of femur shaft, 4-point ultimate breaking strength (displacement rate = 3.0 mm/minute) was measured using an Instron 5500 Testing

Unit at Numira Biosciences. The femora were mounted with a 2.5 mm inner support and a 7.0 mm outer support.

Plasmids. Plasmids encoding human BMP2, human sFrp4 and the Id1-luciferase reporter construct were previously reported ⁵⁻⁷. *Ex vivo* and *in vitro* studies were independently performed and independently repeated by the first authors and co-authors.

Isolation of calvarial- and bone marrow-derived osteoblasts. Calvariae were dissected from 1 to 3 day-old neonatal mice and sequentially digested for 15 min in α -MEM containing 0.1% collagenase and 0.2% dispase (Roche). Calvarial-derived osteoblasts (cOBs) obtained from fractions 2-6 were expanded in culture as described below. Long bones (tibia and femur) from 10 week-old mice were capped below the growth plate at the proximal and distal end. Bone marrow was flushed with α -MEM containing 20% FBS and 100 units/ml penicillin and 100 μ g/ml streptomycin (Invitrogen). Bone marrow osteoblasts (bmOBs) were allowed to adhere overnight, followed by replacement of the tissue culture medium as described below.

Cell culture. Calvarial-derived osteoblasts (cOBs), bone marrow-derived osteoblasts (bmOBs), and MC3T3-E1 cells were cultured in α -MEM supplemented with 10% fetal bovine serum (FBS) and 100 units/ml penicillin and 100 μ g/ml streptomycin. To induce osteogenic differentiation of primary calvarial osteoblasts and of bone marrow stromal cells, medium was supplemented with 5 mM β -glycerolphosphate (Calbiochem), 50 μ M ascorbic acid, and 10 nM dexamethasone (Sigma-Aldrich) for the time indicated.

Real Time PCR. Total RNA was isolated from cells using the RNeasy Mini Kit (Qiagen) according to the manufacturer's protocols. Total RNA from cortical bone of *wt* and *Sfrp4* null mice was extracted using Trizol reagent (Invitrogen) followed by RNeasy Mini Kit

(Qiagen) according to the manufacturer's protocols. cDNA was synthesized using SuperScript VILO (Invitrogen). Quantitative real time PCR was performed using using an iCycler (BioRad). mRNA levels encoding each gene of interest were normalized for GAPDH or actin mRNA in the same sample and the relative expression of the genes of interest was determined using using the formula of Livak and Schmittgen ⁸. cOB and bmOB from at least three distinct litters were used. Data are presented as fold change relative to *wt* cells.

Immunocytochemistry. cOBs isolated from *Sfrp4*^{-/-} mice and *wt* littermates were cultured for 5 days under osteogenic conditions and than fixed with 3.7% formaldehyde. Cells were immune-stained with rabbit polyclonal anti-phospho-Smad1/5/8 antibody (Cell signaling) at a 1:100 dilution and Alexa Fluor fluorescent conjugated secondary antibody (Molecular Probes). ToPro (Molecular Probes) was used at a 1:1.000 dilution for nuclear labeling. Images were obtained at room temperature using a laser-scanning microscope (LSM 510 Meta; Carl Zeiss) equipped with a Plan Neofluar 63x/1.4 NA water immersion lens and Zeiss LSM 510 software. To prevent interference between fluorochromes, each channel was imaged sequentially using the multi-track recording module before merging. Total enhancements were performed using Photoshop (CS2; Adobe).

Gene transfection and luciferase reporter assay. Cells were transfected with FuGENE 6 transfection reagent (Roche) according to the manufacturer's recommendation. Cells were transfected with the Id1-luc reporter plasmid (30ng), human sFrp4 (60ng), Wnt5a (60ng) or human BMP2 (60ng) plasmids. pCMV-Renilla-luciferase (8 ng) was used for normalization. In all transfection assays, empty vector DNA was used to equalize the total amount of DNA. After 3h of transfection, MC3T3-E1 cells were incubated with or without 100 ng/ml of the soluble BMP type1A receptor antagonist RAP-661 (Acceleron Pharma), 1 μ g/ml Noggin (R&D) or 100 nM of the JNK phosphorylation inhibitor SP600125 (Tocris). Luciferase

activity was determined 24h after stimulation using the dual-luciferase reporter assay (Promega) as described by the manufacturer and normalized by Renilla-firefly activity.

Western analysis. 10 µg of protein were resolved by SDS-PAGE under reducing conditions. Immunodetection was performed with anti-active β-Catenin (non-phospho-β-catenin ser33/37/Thr41) antibody, anti-JNK antibody, phospho-JNK (Thr183/Tyr185) antibody, anti-phospho-Smad 1-5-8 antibody and anti-Smad1 antibody (all from Cell Signaling), or anti-Actin antibody (Chemicon International). Immunoreactive proteins were visualized using enhanced chemiluminescence system (Amersham Biosciences), according to the manufacturer's instructions. Films were scanned (scanjet 5530; Hewlett-Packard) and saved as eight bits gray scale image (photosmart studio software; Hewlett-Packard). Fold changes were assessed using Image J. (<http://imagej.nih.gov/ij/>). cOBs and bmOBs from at least three animals from distinct litters were used.

BMP inhibitor (Soluble BMP type 1A compound, RAP-661) treatment. *wt* and *Sfrp4^{+/-}* males were divided into 4 groups of 4 mice each: vehicle-treated *wt* mice, RAP-661-treated *wt* mice, vehicle-treated *Sfrp4^{+/-}* mice, and RAP-661-treated *Sfrp4^{+/-}* mice. Treatment with vehicle (PBS) or RAP-661 (10 mg/kg, Acceleron Pharma) was started at 1 week of age every day for 2 weeks^{9,10}. Mice were sacrificed at 3 weeks of age. Tibiae were collected and analyzed by histomorphometry as described above.

Sclerostin neutralizing antibody treatment. *Wt* and *Sfrp4^{-/-}* mice were divided into four groups: vehicle-treated *wt* mice, sclerostin antibody-treated *wt* mice, vehicle-treated *Sfrp4^{-/-}* mice, and sclerostin antibody-treated *Sfrp4^{-/-}* mice (3-5 mice/group). Treatment with vehicle (phosphate buffered saline) or sclerostin neutralizing antibody (preclinical Scl-AbVI, 25mg/kg, Amgen Inc.) was done at 4 weeks of age twice a week for 3 weeks. Mice were

sacrificed at 7 weeks of age. Tibiae were collected and bone histomorphometry analysis performed as described above.

Statistical analysis. Mean values and the standard deviation (SD) or the standard error of the mean (SEM) were calculated. To determine significant differences, the means of all groups were first analyzed by analysis of variance. If a F-test yielded significant results ($P < 0.05$), groups were compared using Fisher's protected least significant difference post hoc test. Calculations were carried out using the StatView 4.1 statistic analysis software (SAS Institute). P values less than 0.05 were considered significant.

SUPPLEMENTARY FIGURES AND TABLES



Figure S1. Appearance and skeletal radiographs of patients 2, 3 and 4.

A. Patient 2, a 14-year-old girl, showing slender body habitus with moderate valgus deformity at the elbows and mild valgus deformity at the knees. Her stature was 172 cm (above the 97th percentile for Turkish girls). **B.** Patient 4, a 3 7/12 year-old boy, showing marked valgus deformity at the knees. His height of 89 cm was at the 10th percentile. Compare with the photograph of patient 1 (Fig. 1). **C, D.** Skeletal radiographs of patient 2 show expanded metaphyses with lack of modeling, very thin cortex, particularly visible at the distal femurs and proximal tibia. In C, note the normal cortical thickness in the middle part of the femoral diaphysis (see discussion). In D, note incurvation of the tibia. See also patient 2's hand radiographs in Fig 1C. **E, F and G.** Radiographs of patient 4 at age 3 7/12 years. In E, note the chalk-like appearance of the bone with expanded metaphyses and thin cortex. In F, genu valgum deformity; in G, the metaphyseal widening of distal radius and ulna and the widened phalanges. **H.** Radiograph of the hands of patient 3, a 58-year-old man. The distal radius and ulna show the wide metaphyses with thin cortices. The metacarpal and phalanges are undertubulated.



Figure S2. Radiographs of the clinically unaffected brother (age 7 yrs; A, B, C) and father (age 39 yrs; D and E) who are heterozygous for the *SFRP4* c.498_499insG mutation. There is undermodeling visible at the distal tibia (B, D) and distal radius (C,E) as well as mild incurvation of the tibia (B,D). This is compatible with a mild expression of the heterozygous state, as has been observed in other families.

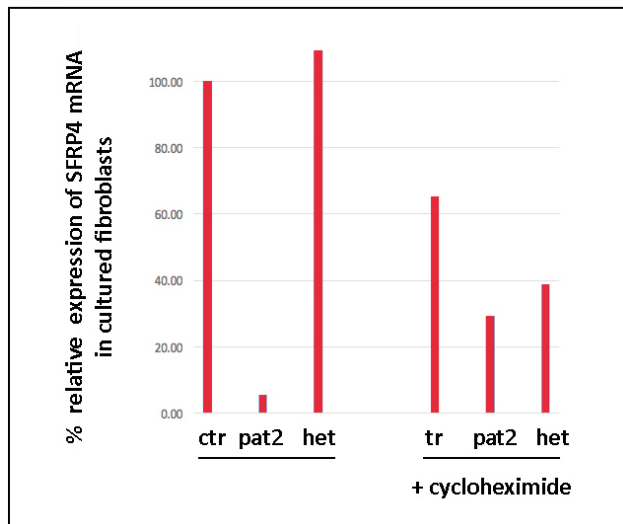


Figure S3. Quantification of SFRP4-specific mRNA in cultured fibroblasts isolated from patient 2. Total RNA from confluent fibroblast cultures was purified and retrotranscribed, and cDNA-specific (exon spanning) primers were used to amplify segments of the *SFRP4* and of the *GAPDH* cDNAs in a qPCR machine. The *SFRP4/GAPDH* ratio in control cells was set as 100% and the results expressed as percent compared to the reference value. Under native culture conditions, the expression of *SFRP4* in cells from patient 2 are significantly lower than in cells from a control subject or from her heterozygous (unaffected) younger brother. In presence of cycloheximide, an inhibitor of nonsense-mediated mRNA decay, the *SFRP4* mRNA levels in the patient increase to approach those in the other cell lines.

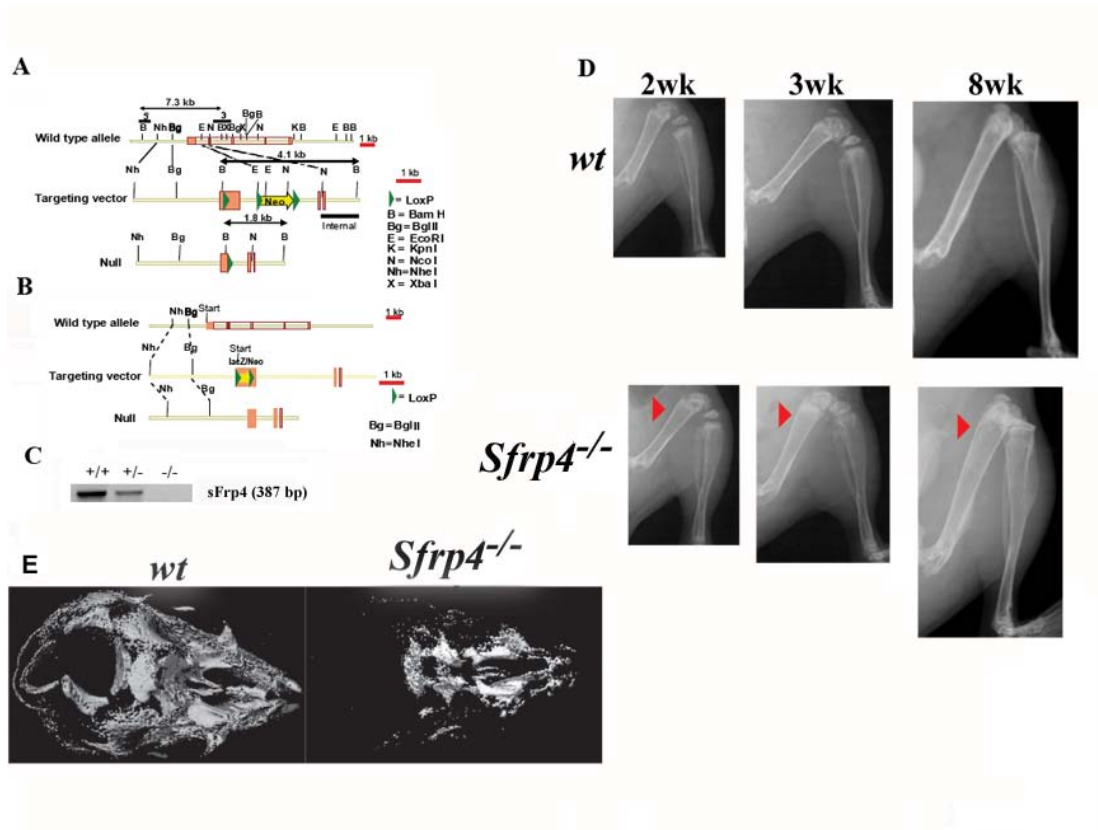


Figure S4. Generation of *sFrp4* null mice and their characterization. **A.** Partial restriction maps of the wt *Sfrp4* gene locus, the targeting vector, and the disrupted *Sfrp4* allele for mice generated at Procter & Gamble. The exon 1 coding region of the *sFrp4* gene was replaced by a neomycin (neo) cassette. B, Bam H1; Bg, Bgl2; E, EcoR1; K, Kpn1, N, Nco1; Nh, Nhe1; S, Sal1; X, Xba1. PCR products of the wt, the *Sfrp4*^{+/-}, and the *Sfrp4*^{-/-} genotype are shown in the right top. **B.** Knockout strategy of *sFrp4* null mice generated at Lexicon. **C.** PCR products of wt, *Sfrp4*^{+/-}, and *Sfrp4*^{-/-} are shown. **D.** Representative radiographic images of wt and *Sfrp4*^{-/-} female littermates at different time points. Arrows indicate the expanded metaphyses in the null mice ($n=4$). **E.** Representative μ CT images of whole head of neonatal wt and *Sfrp4*^{-/-} mice at day 2 of age.

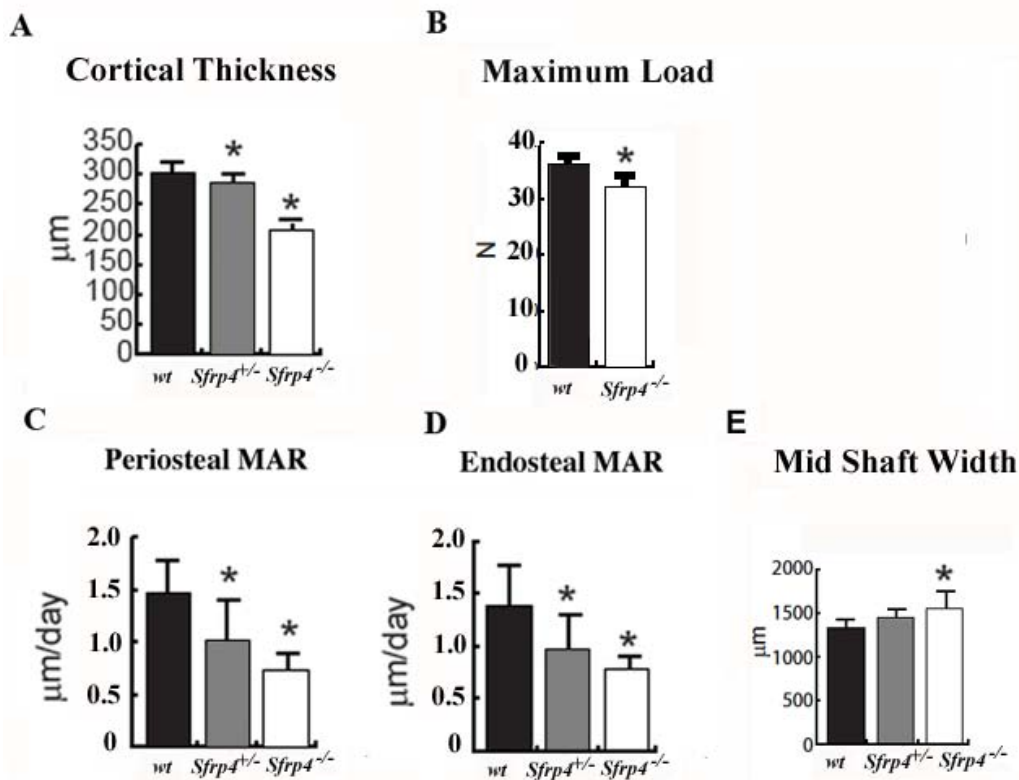


Figure S5. Effect of *Sfrp4* deletion on cortical bone. **A.** Measurement of the cortical thickness in 10-weeks old tibiae isolated from *wt*, *Sfrp4*^{+/-}, and *Sfrp4*^{-/-} mice using bone histomorphometry (*n*=5). Data are shown as the mean ± SEM. *; *P*<0.05 vs. *wt* littermates. **B.** Four-point bending maximum load in femur of 24-weeks *wt* and *Sfrp4*^{-/-} female mice. Data are mean ± SEM. *=*P*<0.05 vs. *wt* littermates. (*n*=9). **C and D.** Mineral Apposition Rate (MAR) at the periosteum (C) and at the endosteum (D) of the cortical bone of 10-weeks old tibiae isolated from *wt*, *Sfrp4*^{+/-}, and *Sfrp4*^{-/-} mice using bone histomorphometry (*n*=5). Data are shown as the mean ± SEM. *; *P*<0.05 vs. *wt* littermates. **E.** Quantification of the mid-shaft width in tibiae of 10-weeks old *wt*, *Sfrp4*^{+/-}, and *Sfrp4*^{-/-} mice using bone histomorphometry (*n*=5). Data are expressed as mean ± SEM. *; *P*< 0.05 vs. *wt* littermates.

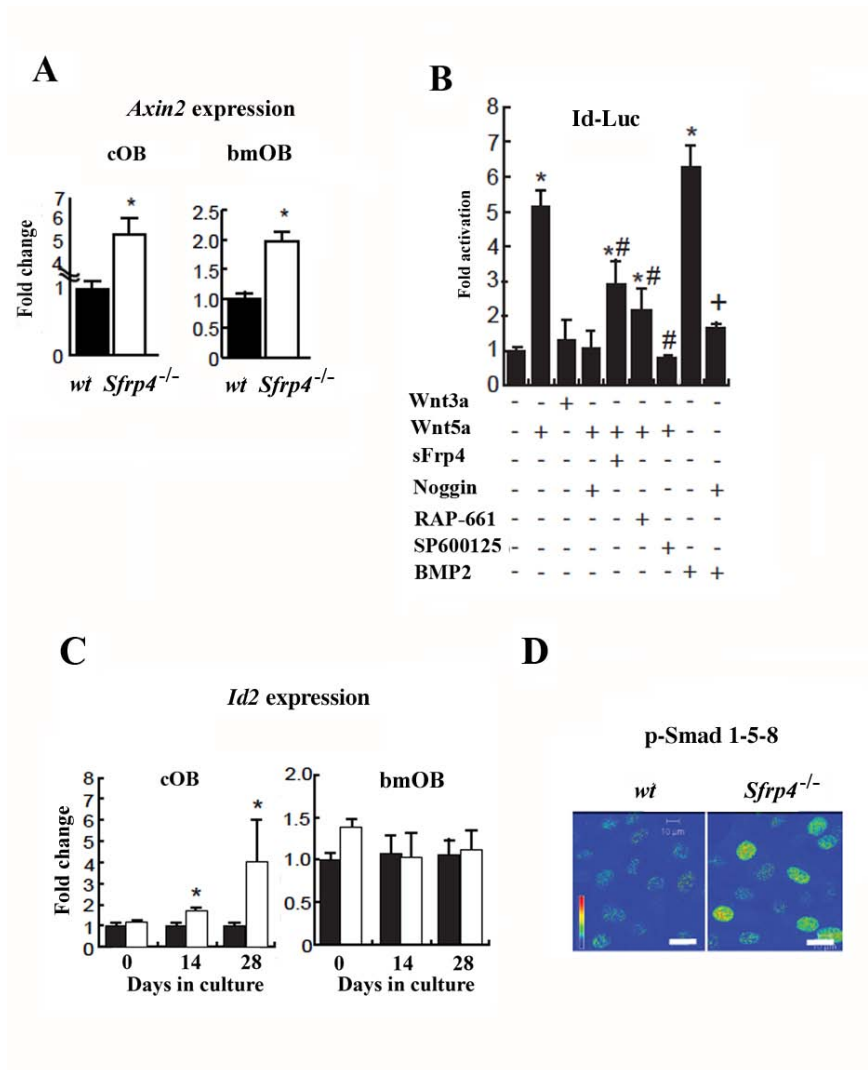


Figure S6. sFrp4 regulation of canonical Wnt and BMP signaling. **A.** Quantification of *Axin2* mRNA expression in *wt* and *Sfrp4*^{-/-} cOBs and bmOBs. Data are shown as mean ± SD. *; P<0.05 vs *wt* cells at each time point (*n*=3). **B.** MC3T3-E1 cells transiently transfected with a plasmid encoding the BMP-responsive Id-luciferase reporter gene were co-transfected with plasmids encoding Wnt3a, Wnt5a, and BMP2 or stimulated with exogenously administered sFrp4, Noggin, SP600125 or RAP-661. Data are shown as mean ± SD. *; P<0.05 vs control, #; P<0.01 vs Wnt5a stimulation, +; P<0.05 vs. BMP stimulation (*n*=3). **C.** Quantification of *Id2* mRNA expression in *wt* (black bars) and *Sfrp4*^{-/-} (open bars) cOBs and bmOBs. Data are shown as mean ± SD. *; P<0.05 vs *wt* cells at each time point (*n*=3). **D.** Representative images of immunocytochemistry of phosphorylated Smad1/5/8 in *wt* and *Sfrp4*^{-/-} cOBs (*n*=3).

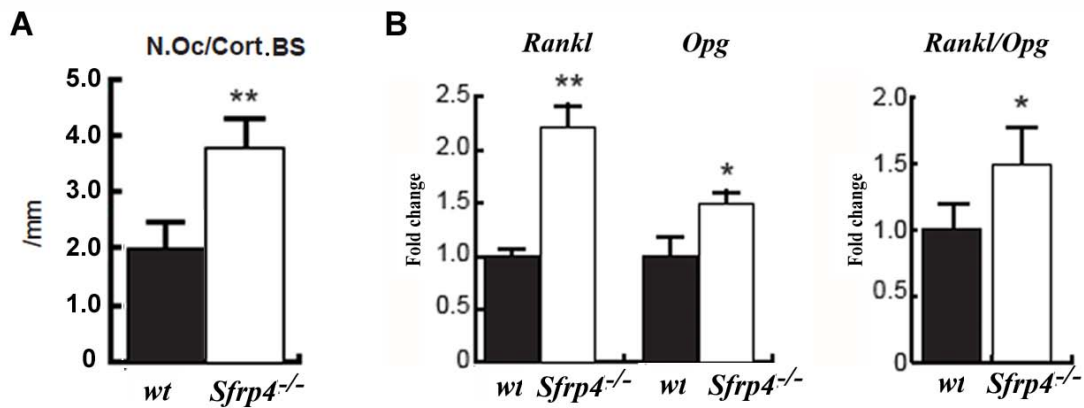


Figure S7. Effect of *sFrp4* deletion on endocortical osteoclasts and RANKL and OPG expression in cortical bone. **A.** Histomorphometric analysis of the number of osteoclasts at the endocortical bone surface (N.Oc/Cort.BS) in tibiae isolated from *wt* and *Sfrp4*^{-/-} mice. Data are mean ± SD. **, P<0.01 vs *wt* mice (n=5). **B.** Quantification of *Rankl* and *Opg* mRNA expression and calculation of the *Rankl/Opg* ratio in the cortical bone of *wt* and *Sfrp4*^{-/-} mice. Data are mean ± SD. *, P<0.05 and **, P<0.01 vs *wt* mice (n=3).

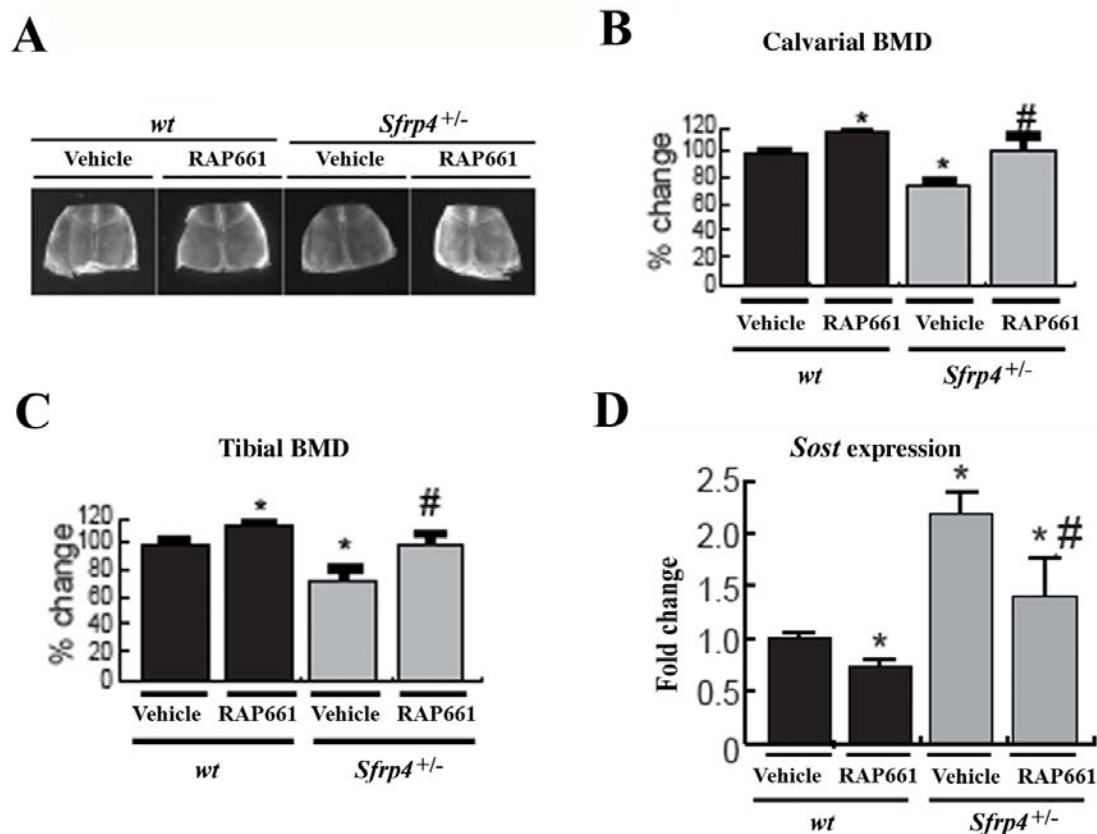


Figure S8. RAP-661 treatment *in vivo*. **A.** Representative X-ray of *wt* and *Sfrp4*^{+/-} calvariae treated with or without RAP-661. **B and C.** Quantification of Bone Mineral Density (BMD) of the calvarial bone (B) and the tibial mid-shaft region (C) of vehicle-or RAP-661-treated *wt* and *Sfrp4*^{+/-} mice. **D.** *Sost* mRNA expression in bones of *wt* and *Sfrp4*^{+/-} mice after treatment with vehicle or RAP-661. Data are mean \pm SEM. *, $P < 0.05$ vs vehicle-treated *wt* mice, #; $P < 0.05$ vs. vehicle-treated *Sfrp4*^{+/-} mice. ($n = 4$).

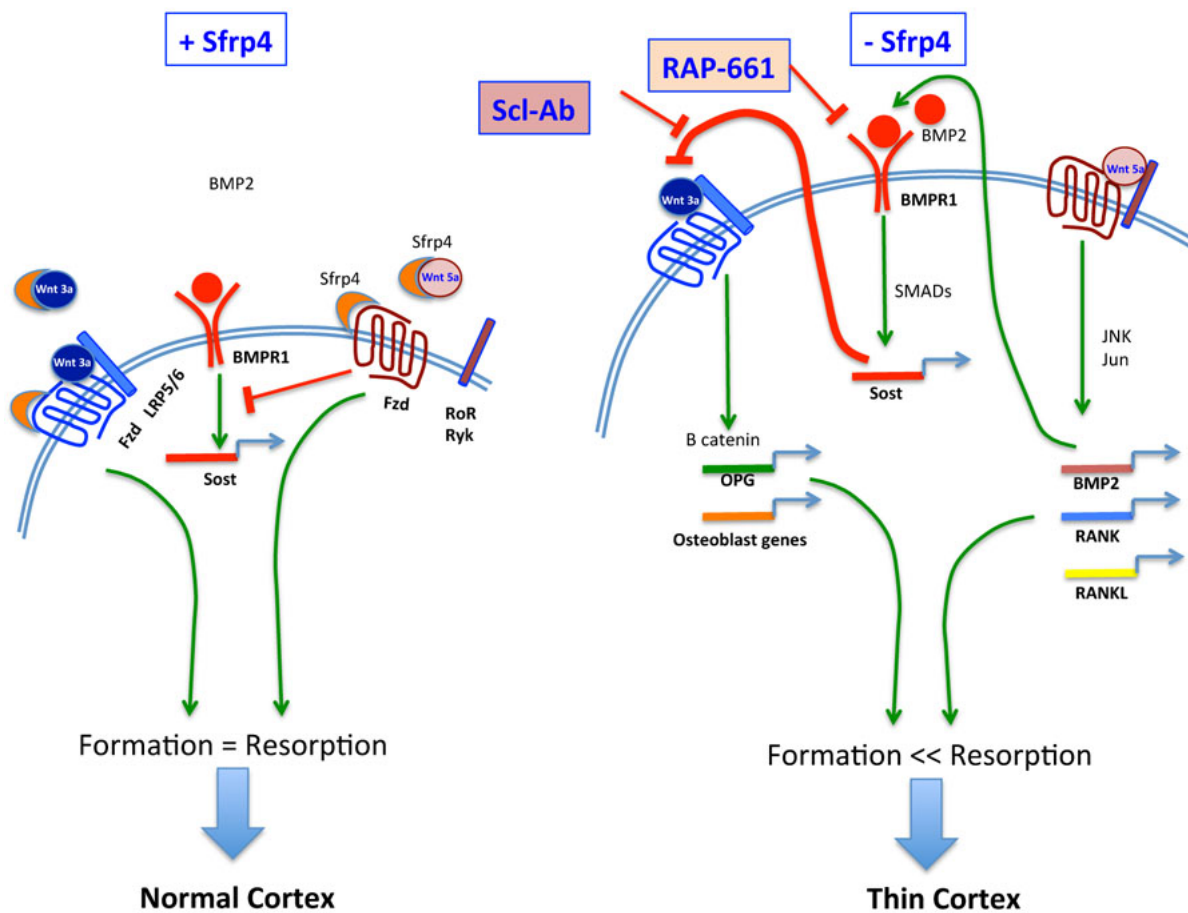


Figure S9. Schematic description of the signaling events under steady state in the cortex in the presence (Left) of absence (as in Pyle disease, Right) of sFrp4: **Left:** In the presence of sFrp4 and equilibrium exists between canonical and non-canonical Wnt signaling, ensuring a balance between bone formation and resorption. **Right:** In the absence of Sfrp4, Canonical Wnt signaling is activated, favoring bone formation over bone resorption, but strong activation of non-canonical Wnt signaling in cortical bone enhances sclerostin production via BMP, repressing bone formation, and induces resorption through expression of RANK²⁵ and RANKL, leading to cortical thinning. Treatment with the BMP signaling inhibitor RAP-661 or with sclerostin antibodies (Scl-Ab) prevent cortical thinning by shutting off the BMP-sclerostin loop preventing thinning of the cortex by balancing bone formation and resorption. Fzd= Frizzled receptors; LRP5/6= Wnt canonical co-receptors; Ror, Ryk= Wnt non-canonical co-receptors; BMPR1= BMP receptors type 1; OPG= Osteoprotegerin.

Table S1. Markers of bone metabolism in plasma. Reference ranges (*rr*) are matched for gender and age range.

		control (adult)	II-1 (16yrs)	II-2 (14yrs)	II-3 (7yrs)	I-1 (adult)	I-2 (adult)
CTX	units ng/ml	0.342	1.32	1.65	1.27	0.098	0.184
Osteocalcin	ng/ml	23.3 <i>(rr:13.5-160.1)</i>	160.1 <i>(rr: 32-124.2)</i>	184.8 <i>(rr: 15.4-88.8)</i>	78.92 <i>(rr: 12.5-232.5)</i>	14.9 <i>(rr: 13.5-160.1)</i>	18.84 <i>(rr: 20.7-45.6)</i>
Bone-specific alkaline phosphatase	ng/ml	n/a	>75 <i>(rr: 13-80)</i>	>75 <i>(rr: 12.6.- 105.8)</i>	>75 <i>(rr: 51-164)</i>	14.8 <i>(rr: <14)</i>	18.2 <i>(rr: < 20)</i>
PINP	ng/ml	48.45 <i>(rr: 38.7-494.5)</i>	1035 <i>(rr: 77.7-430.3)</i>	717.6 <i>(rr: 58.5-451)</i>	566.4 <i>(rr 9-10 yrs: 45.2-552.5)</i>	28.4 <i>(rr 38.7-494.5)</i>	49.5 <i>(rr: 36.3-143.9)</i>
OPG	pmol/l	2.65	2.95	3.43	3.63	4.07	2.9
Sclerostin	pmol/l	66	50.5	55.3	59.4	61.8	52.2

Table S2. Overview of the filtering of exonic and splicing variants observed in the patients.

	Pat.1	Pat. 2
Number of exonic and splicing variants	23193	22621
Number of non-synonymous variants	11593	11272
Number of rare variants (<1%)	720	710
Number of rare variants after quality control (QC)	360	358
Number of genes with homozygous variants	34	26
+ in homozygous regions	16	15
+ in common	11	
+ Variants affecting conserved amino acid	3	

Table S3. Proximal tibial metaphyseal trabecular bone histomorphometry of 10- and 44-week old *wt*, *Sfrp4^{+/-}* and *Sfrp4^{-/-}* males

10 weeks

Parameters	<i>wt</i> (n=5)	<i>Sfrp4^{+/-}</i> (n=5)	<i>Sfrp4^{-/-}</i> (n=5)
BV/TV (%)	11.26±5.8	15.77±3.8*	36.42±7.0**#
Tb.Th (µm)	40.4±5.7	44.6±7.7NS	69.2±12.7*#
Tb.N (/mm)	2.70±1.27	3.47±0.30 *	5.28±0.56**#
Tb.Sp (µm)	496.3±478	245.0±31*	121.6±19**#
MS/BS (%)	24.7±8.4	32.6±4.1NS	31.6±11.8NS
MAR (µm/day)	2.11±0.3	2.34±0.1*	2.60±0.2*
BFR/TV (%/year)	93.2±45.3	193.7±26.0 *	313.6±113.23**#
Ob.S/BS (%)	12.5±1.2	17.4±2.8*	25.9±3.1*
N.Ob/B.Pm (/mm)	6.0±0.4	8.3±2.3*	12.8±1.8*
OS/BS (%)	3.0±0.6	2.3±0.4NS	2.5±0.4NS
Oc.S/BS (%)	0.55±0.1	0.63±0.1NS	0.70±0.1NS
N.Oc/B.Pm (/mm)	0.94±0.2	0.64±0.3NS	0.58±0.1NS
ES/BS (%)	0.82±0.3	0.71±0.1NS	0.92±0.1NS

44 weeks

Parameters	<i>wt</i> (n=5)	<i>Sfrp4^{+/-}</i> (n=5)	<i>Sfrp4^{-/-}</i> (n=5)
BV/TV (%)	4.6±5.2	9.2±3.2	16.4±7.2 *
Tb.Th (µm)	28.3±9.3	41.8±8.7	54.2±21.8*
Tb.N (/mm)	1.3±1.1	2.1±0.3	3.0±0.2*
Tb.Sp (µm)	988.9±515	424.7±69*	280.2±41**
MS/BS (%)	9.1±5.0	19.2±6.6	21.1±9.8*
MAR (µm/day)	0.76±0.6	2.1±0.2**	2.03±0.3**
BFR/TV (%/year)	7.4±2.5	63.5±16.3*	94.7±43.7**
Ob.S/BS (%)	4.9±1.7	13.1±4.9*	17.7±5.7**
N.Ob/B.Pm (/mm)	2.6±0.7	6.9±2.9*	8.1±2.1**
OS/BS (%)	1.0±0.64	2.6±1.6NS	1.5±0.6NS
Oc.S/BS (%)	0.66±0.4	0.50±0.2NS	0.45±0.2NS
N.Oc/B.Pm (/mm)	0.65±0.4	0.42±0.1NS	0.38±0.1NS
ES/BS (%)	0.91±0.5	0.72±0.3NS	0.85±0.3NS

*: P<0.05 vs. WT, **: P<0.01 vs. WT, #: P<0.05 vs. *Sfrp4^{+/-}* and NS: Not significant

Table S4. Bone histomorphometry of *wt*, and *Sfrp4*^{+/-} treated with RAP661 or vehicle

Parameters	<i>wt</i> +Vehicle	<i>wt</i> +RAP661	<i>Sfrp4</i> ^{+/-} +Vehicle	<i>Sfrp4</i> ^{+/-} +RAP661
	(n= 4)	(n= 4)	(n= 4)	(n= 4)
BV/TV (%)	7.32±0.79	12.27±2.26	11.9±1.02	17.37±2.35
Tb.Th (µm)	30.8±1.3	40.9±7.4	42.87±4.9	48.27±5.3
Tb.N (/mm)	2.36±0.37	2.96±0.42	2.78±0.1	3.6±0.69
Tb.Sp (µm)	398.7±62.6	300.12±55.5	317.0±17.05	237.66±56.09
MS/BS (%)	21.45±0.6	30.6±3.2	31.07±3.0	32.5±2.03
MAR (µm/day)	1.03±0.06	1.83±0.12	1.84±0.13	2.44±0.24
BFR/BS (µm ³ /µm ² /year)	80.8±29.9	208.23±35.07	209.36±36.22	290.55±36.8
BFR/BV (%/year)	406.0±48.3	999.7±123.3	983.6±157.4	1233.7±187.1
BFR/TV (%/year)	58.7±0.64	144.99±25.45	140.82±43.8	258.33±36.6
Ob.S/BS (%)	13.0±1.3	19.7±1.8	18.0±1.6	29.3±4.1
N.Ob/B.Pm (/mm)	7.3±0.57	10.9±0.8	10.5±1.1	17.8±2.5
OS/BS (%)	11.8±1.0	18.7±1.6	16.8±1.52	29.8±5.0
OV/BV (%)	1.61±0.26	2.47±0.39	2.54±0.48	2.69±0.54
Oc.S/BS (%)	0.92±0.12	0.50±0.12	0.54±0.06	0.33±0.04
N.Oc/B.Pm (/mm)	0.39±0.02	0.23±0.38	0.24±0.10	0.56±0.10
ES/BS (%)	1.02±0.13	0.57±0.13	0.60±0.07	0.40±0.04
Femur Bone diameter (µm)	745±80	746±70	934±112	778±82
Endocort MAR (µm/day)	2.40±0.17	1.13±0.24	3.79±0.66	2.17±0.21
Cortical thickness (µm)	230.0±9.8	344.6±9.2	201.7±11.3	275.3±19.2

Parameters	P value <i>wt</i> Vehicle vs. <i>Sfrp4</i> ^{+/-} vehicle	P value <i>wt</i> RAP661 vs. <i>Sfrp4</i> ^{+/-} RAP661	P value, <i>wt</i> Vehicle vs. <i>wt</i> RAP661	P value <i>Sfrp4</i> ^{+/-} Vehicle vs. <i>Sfrp4</i> ^{+/-} RAP661	P value <i>wt</i> Vehicle vs. <i>Sfrp4</i> ^{+/-} RAP661
BV/TV (%)	0.013	0.10	0.06	0.036	0.005
Tb.Th (µm)	0.023	0.11	0.045	0.115	0.003
Tb.N (/mm)	0.092	0.15	0.086	0.030	0.015
Tb.Sp (µm)	0.072	0.13	0.094	0.048	0.012
MS/BS (%)	0.010	0.33	0.065	0.32	0.0053
MAR (µm/day)	0.0003	0.042	0.019	0.039	0.0043
BFR/BS (µm ³ /µm ² /year)	0.0043	0.073	0.056	0.078	0.0050
BFR/BV (%/year)	0.0012	0.15	0.048	0.17	0.0099
BFR/TV (%/year)	0.0059	0.040	0.11	0.024	0.0061
Ob.S/BS (%)	0.023	0.005	0.042	0.46	0.048
N.Ob/B.Pm (/mm)	0.035	0.039	0.067	0.22	0.052
OS/BS (%)	0.031	0.063	0.058	0.37	0.049
Oc.S/BS (%)	0.096	0.174	0.211	0.022	0.079
N.Oc/B.Pm (/mm)	0.182	0.108	0.256	0.001	0.103
ES/BS (%)	0.095	0.182	0.243	0.020	0.078
Bone diameter (µm)	0.0025	0.23	0.95	0.0017	0.28
Endocort MAR (µm/day)	0.0026	0.081	0.05	0.046	0.135
Cortical thickness (µm)	0.002	0.013	0.0003	0.013	0.048

Table S4. Bone histomorphometry analysis of proximal tibial metaphyseal trabecular of *wt* and *Sfrp4*^{+/-} treated with vehicle or RAP-661. Data are mean ± SEM.

Table S5. Bone histomorphometry of *wt* and *Sfrp4*^{+/-} treated with Scl-Ab or vehicle

Parameters	<i>wt</i> +Vehicle (n= 5)	<i>wt</i> +Scl-Ab (n= 4)	<i>Sfrp4</i> ^{+/-} +Vehicle (n= 5)	<i>Sfrp4</i> ^{+/-} +Scl-Ab (n= 3)
BV/TV (%)	7.7±1.2	14.0±1.1	11.8±1.0	26.9±2.9
Tb.Th (µm)	32.5±2.6	43.7±3.1	29.4±1.8	59.4±1.9
Tb.N (/mm)	2.3±0.2	3.2±0.3	4.0±0.1	4.5±0.4
Tb.Sp (µm)	418.5±55.2	273.8±28	222.3±9.4	167.0±21
MS/BS (%)	34.5±2.9	52.6±1.1	34.6±1.65	49.0±1.14
MAR (µm/day)	1.47±0.13	2.48±0.08	1.96±0.06	2.40±0.2
BFR/BS (µm ³ /µm ² /year)	189.0±29.9	477.03±22.9	249.3±19.0	430.0±35.8
BFR/BV (%/year)	768.8±88.5	1617.8±108	1401.0±179.9	1162.0±117.3
BFR/TV (%/year)	118.6±23.7	399.3±27.9	201.3±19.7	380.3±44.4
Ob.S/BS (%)	11.09±3.5	25.26±1.19	21.16±1.74	21.33±0.66
N.Ob/B.Pm (/mm)	7.0±2.24	14.54±0.66	12.2±1.1	13.24±0.45
OS/BS (%)	10.8±3.7	24.31±1.0	21.16±1.21	21.33±1.54
Oc.S/BS (%)	0.78±0.25	0.30±0.06	0.53±0.08	0.23±0.05
N.Oc/B.Pm (/mm)	0.39±0.14	0.21±0.08	0.27±0.01	0.12±0.02
ES/BS (%)	0.82±0.25	0.34±0.07	0.61±0.09	0.28±0.05
Bone diameter (µm)	1498±49	1594±73.9	1872±89	1659±14.7
Endocort MAR (µm/day)	3.53±0.09	6.87±0.48	2.51±0.40	5.25±0.39
Cortical thickness (µm)	232±4.5	316.5±10.8	172.8±3.2	321±22.9

Parameters	P value <i>wt</i> Vehicle vs. <i>Sfrp4</i> ^{+/-} Vehicle	P value <i>wt</i> Scl-Ab vs. <i>Sfrp4</i> ^{+/-} Scl-Ab	P value <i>wt</i> Vehicle vs. <i>wt</i> Scl- Ab	P value <i>Sfrp4</i> ^{+/-} Vehicle vs. <i>Sfrp4</i> ^{+/-} Scl- Ab	P value <i>wt</i> Vehicle vs. <i>Sfrp4</i> ^{+/-} Scl-Ab
BV/TV (%)	0.016	0.025	0.0036	0.019	0.009
Tb.Th (µm)	0.17	0.005	0.015	0.0001	0.0001
Tb.N (/mm)	0.0005	0.035	0.0005	0.17	0.007
Tb.Sp (µm)	0.011	0.017	0.011	0.068	0.0038
MS/BS (%)	0.48	0.038	0.002	0.0001	0.0056
MAR (µm/day)	0.012	0.37	0.0005	0.071	0.0096
BFR/BS (µm ³ /µm ² /year)	0.074	0.16	0.0001	0.009	0.0026
BFR/BV (%/year)	0.011	0.019	0.0005	0.15	0.0027
BFR/TV (%/year)	0.027	0.36	0.0001	0.019	0.0069
Ob.S/BS (%)	0.024	0.06	0.013	0.049	0.024
N.Ob/B.Pm (/mm)	0.026	0.05	0.006	0.041	0.024
OS/BS (%)	0.014	0.075	0.008	0.057	0.033
Oc.S/BS (%)	0.017	0.12	0.024	0.024	0.003
N.Oc/B.Pm (/mm)	0.005	0.075	0.018	0.016	0.001
ES/BS (%)	0.013	0.154	0.022	0.032	0.003
Bone diameter (µm)	0.0078	0.23	0.17	0.047	0.014
Endo cort MAR (µm/day)	0.0007	0.024	0.0026	0.0061	0.021
Cortical thickness (µm)	0.0009	0.42	0.0010	0.010	0.027

Table S5. Bone histomorphometry analysis of proximal tibial metaphyseal trabecular of *wt* and *Sfrp4*^{+/-} treated with vehicle or Scl-Ab. Data are mean ± SEM.

SUPPLEMENTARY REFERENCES

1. Van der Auwera GA, Carneiro MO, Hartl C, et al. From FastQ data to high confidence variant calls: the Genome Analysis Toolkit best practices pipeline. *Curr Protoc Bioinformatics* 2013;11:11 0 1- 0 33.
2. Wang K, Li M, Hakonarson H. ANNOVAR: functional annotation of genetic variants from high-throughput sequencing data. *Nucleic Acids Res* 2010;38:e164.
3. Seelow D, Schuelke M, Hildebrandt F, Nurnberg P. HomozygosityMapper--an interactive approach to homozygosity mapping. *Nucleic Acids Res* 2009;37:W593-9.
4. Parfitt AM, Drezner MK, Glorieux FH, et al. Bone histomorphometry: standardization of nomenclature, symbols, and units. Report of the ASBMR Histomorphometry Nomenclature Committee. *J Bone Miner Res* 1987;2:595-610.
5. Sabatakos G, Rowe GC, Kveiborg M, et al. Doubly truncated FosB isoform (Delta2DeltaFosB) induces osteosclerosis in transgenic mice and modulates expression and phosphorylation of Smads in osteoblasts independent of intrinsic AP-1 activity. *J Bone Miner Res* 2008;23:584-95.
6. Rattner A, Hsieh JC, Smallwood PM, et al. A family of secreted proteins contains homology to the cysteine-rich ligand-binding domain of frizzled receptors. *Proc Natl Acad Sci U S A* 1997;94:2859-63.
7. Katagiri T, Imada M, Yanai T, Suda T, Takahashi N, Kamijo R. Identification of a BMP-responsive element in Id1, the gene for inhibition of myogenesis. *Genes Cells* 2002;7:949-60.
8. Livak KJ, Schmittgen TD. Analysis of relative gene expression data using real-time quantitative PCR and the 2(-Delta Delta C(T)) Method. *Methods* 2001;25:402-8.

9. Mulivor A. SN, Kawamoto Y. , R. Kumar, J. Seehra, R.S. Pearsall Inhibition of ALK3 (BMPRIA) signaling using RAP-661, a novel bmp antagonist, increases bone mass in ovariectomized mice. *Bone* 2011;48:S98-S9.
10. Solban N. C-BM, Kawamoto Y., Andreucci A., Umiker B.R., Walrond S., Underwood1 K.W., Kumar R., Seehra J., Pearsall R.S. . A soluble BMP antagonist increases bone mass of osteopenic male mice. *Bone* 2010;47:S219.